

Three Degrees-of-Freedom Optical Spindle Error Motion Measurement Device

Hau-Wei Lee,* Jr-Rung Chen,¹ Bing-Lin Ho,¹ and Chi-Chang Wang²

Department of Mechanical Engineering, National Chung Hsing University, Taichung City 402, Taiwan

¹Center for Measurement Standards, International Technology Research Institute, Hsinchu City 300, Taiwan

²Department of Mechanical and Computer-Aided Engineering, Feng-Chia University, Taichung City 407, Taiwan

(Received April 14, 2017; accepted July 25, 2017)

Keywords: spindle, error motion, IoT, autocollimator, standard sphere

An inexpensive optical measurement device for spindle error measurement, which has three degrees of freedom (3DOF) and is integrated with the Internet of things (IoT), is presented. The device uses an artificial standard sphere, which is set on the spindle to be measured, and two optical measurement modules. Each module includes an aspherical lens, a laser diode, a beam splitter and a quadrant position-sensing detector, and the autocollimator principle of measurement is used. After the calibration of the device, the residual error and resolution are about 1 and 0.1 μm , respectively. The experiment results show errors of measurement, caused by the roughness of the standard sphere, as periodic noise with an amplitude of 10 μm . After the noise has been eliminated, the error motion of the spindle, which includes radial, axial, and synchronous and asynchronous errors, can be observed. The proposed device can also be used for the measurement of spindle thermal expansion.

1. Introduction

Spindle error motion measurements have been standardized in the International Organization for Standardization (ISO) 230-7, which includes axial, radial, wobble, and face deviations, as well as synchronous and asynchronous errors. One of the simplest noncontact methods for spindle error motion measurement can be achieved by installing a laser on the spindle.⁽¹⁾ However, the power supply for the laser is a serious problem because it needs to be provided by batteries. This can lead to measurement errors caused by a physically unbalanced installation. However, the power supply problem can be avoided by using a reference object in the form of a cylinder or a sphere fixed to the spindle.^(2–5) Capacitance sensors have been used in some studies of spindle error motion measurement^(2,5,6) and, in others, lasers have been used.^(7,8) Two efficient methods using a laser involve either the use of geometrical optics^(7,9–13) or single or multiple laser interferometers.^(8,14) Laser-interferometer-based measurement methods have a higher resolution and a greater accuracy than those using a geometrical optics setup. A method that combines a laser interferometer with geometrical optics allows three-dimensional measurements to be made using interference fringe deviation.⁽¹⁵⁾ However, in addition to these methods being very expensive for simple spindle measurement application, the rates of image capture and data processing are generally too low for use with spindles rotating at a high speed. A method employing an artificial reference object, such as a sphere or a cylinder, with a ball lens and a plano-concave mirror has been described.^(11,12)

*Corresponding author: e-mail: boomas@ms42.hinet.net
<http://dx.doi.org/10.18494/SAM.2017.1656>

Measurement methods using capacitance sensors have the advantage of high accuracy with nanometer resolution. However, their major contribution towards measurement uncertainty is the need for artificial reference objects that are expensive. Because the roundness error of artificial reference objects is generally larger than the capacitance sensor measurement error, and the radial error for spindles generally is about 3–20 μm , sensor measurement at a submicron resolution is sufficient. Optical spindle error motion measurement, using quadrant position-sensing-detectors and lasers, can determine spindle error motion with a high sampling rate and a submicron resolution. The cost of the setup is also much lower than that for a capacitance sensor arrangement and the setup for measuring spindle motion error is straightforward. In this study, we present such a type of measurement device with three degrees of freedom (3DOF). The device is capable of measuring the radial, axial, and synchronous and asynchronous errors of a rotating spindle, and the measurement signals are captured by an inexpensive Raspberry Pi3 with an analog-to-digital (A/D) converter. This also allows the measurement device to be connected and integrated with the Internet of Things (IoT) by means of Bluetooth technology. The device not only provides motion error measurements, but can also be used for spindle thermal expansion monitoring.^(16–19) However, the proposed measurement method cannot be used for on-line or real-time measurement.⁽²⁰⁾

2. 3DOF Measurement Device

2.1 Device structure

The optical layout of the proposed measurement device is shown in Fig. 1. The device uses an artificial standard (AS) sphere, which is installed on the spindle, and two measurement modules. Each module includes a laser diode (LD) with a wavelength of 633 nm and a power of 2 mW, an OSI Optoelectronics (SPOT-9D) quadrant-position-sensing detector (QPD), a Thorlabs (A280TM-A) aspherical lens (AL), and a 50/50 cube beam splitter (BS). The light emitted from the LD is reflected by the BS and focused by the AL onto the center of the AS. The light reflected from the surface of the sphere AS is projected onto the QPD after returning through the AL and BS. The lens parameters are $R = 13.2245$, $k \cong -0.16$, $A_4 \cong 1.18 \times 10^{-4}$, $A_6 \cong -4.60 \times 10^{-5}$, $A_8 \cong 6.3269738 \times 10^{-6}$, and $A_{10} \cong 3.16 \times 10^{-7}$; the effective focal length is 18.4 mm; the working distance is 17.13 mm and the window thickness t is 0.25 mm. The lens is made of H-LaK54 and the refractive index n_{ALens} is 1.73101 for a wavelength of 633 nm.

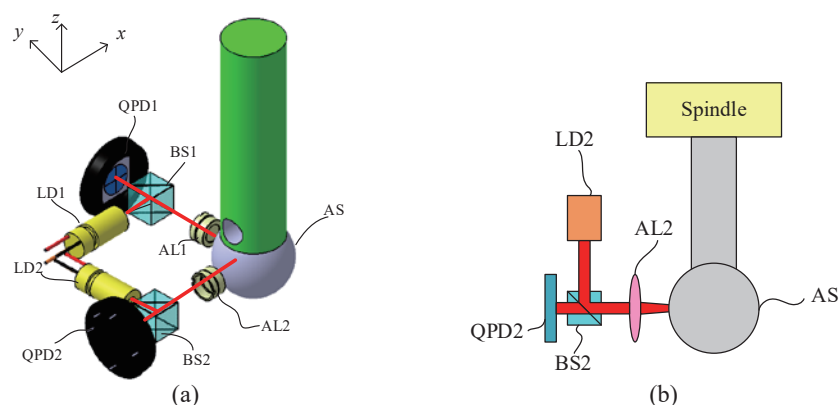


Fig. 1. (Color online) (a) Layout of the 3DOF spindle error motion measurement device and (b) optical path of a sensor setup.

2.2 Measurement principle

The measurement principle of the proposed device is based on the autocollimator concept. As shown in Figs. 1(b) and 2, when the AS moves on the x -axis and is displaced by Δx , the projected spot moves along the x -axis of QPD1 and the spot size on QPD2 changes. When the AS moves along the y -axis, the position of the spot on QPD1 does not change, but on QPD2, it moves horizontally. When the AS moves along the z -axis, the spots on both QPD1 and QPD2 move vertically. The three linear errors can be measured and the relationship between the displacement of the AS and the position of the spots can be derived as

$$\begin{bmatrix} \Delta x \\ \Delta y \\ \Delta z \end{bmatrix} = \begin{bmatrix} k_x & 0 & 0 \\ 0 & k_y & 0 \\ 0 & 0 & k_z \end{bmatrix} \cdot \begin{bmatrix} S_{QPD1,x} \\ S_{QPD2,x} \\ S_{QPD1,y} \end{bmatrix}, \quad (1)$$

where k_x , k_y , and k_z are transformation constants between the AS displacement and the position of the spots; $S_{QPD1,x}$, $S_{QPD1,y}$, and $S_{QPD2,x}$ are the spot positions on QPD1 and QPD2 on the x - and y -axes. Figure 3 shows the mathematical model for a measurement module, in which $\vec{s} = [\Delta x \ \Delta y \ \Delta z]^T$ is the displacement vector of the AS; \vec{r} is the translation vector of the incident light; \vec{p} is the translation vector of the light reflected from the sphere surface; $2\alpha_y$ is the angle between the incident and reflected light; f is the distance from the sphere center to the AL; the scalar r is the radius of the AS; d_{QPDi} is the distance from the AL to the i -th QPD, where $i = 1, 2$. After calculation, linearization, and simplification, the constants k_x , k_y , and k_z can be determined as

$$k_x = 2 \left[\frac{R(t + rn_{ALens} - fn_{ALens}) + d_{QPD1}n_{ALens}(t - R + rn_{ALens} - fn_{ALens})}{rRn_{ALens}} \right], \quad (2)$$

$$k_y = 2 \left[\frac{R(t + rn_{ALens} - fn_{ALens}) + d_{QPD2}n_{ALens}(t - R + rn_{ALens} - fn_{ALens})}{rRn_{ALens}} \right], \quad (3)$$

$$k_z = -2 \left[\frac{R(t + fn_{ALens} - rn_{ALens}) - d_{QPD1}n_{ALens}(t - R + fn_{ALens} - rn_{ALens})}{rRn_{ALens}} \right]. \quad (4)$$

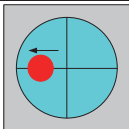
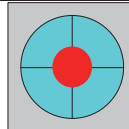
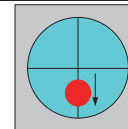
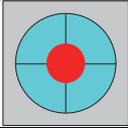
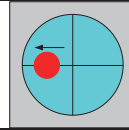
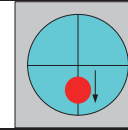
Error Motion	Δx	Δy	Δz
QPD1			
QPD2			

Fig. 2. (Color online) Relationship between laser spot deviation and spindle error motion.

2.3 Signal processing scheme

The most important components for the proposed error measurement device are the AS sphere, sensor modules, and signal processor. The performance of the signal processor determines such things as the maximum sampling rate, the stability of the sampling interval, and the measurement resolution and precision. Usually, a PC-based A/D converter with a sampling rate higher than 100 kHz is not inexpensive and is difficult to use in measurements with the IoT technique. However, in this study, a Raspberry Pi3 was used to collect measurement data. In this manner, we enabled the use of the equipment as an IoT device capable of remote measurement and also kept the cost down. The signal processing schematic is shown in Fig. 4. The measurement device is operated by a PC and the operation commands, and the measurement data is transferred through a Bluetooth interface. The only power cable used is connected to the measurement device and multidevice operation can be carried out. The measurement signal was captured by a Microchip MCP3304 A/D converting IC and the measurement data was recorded by the Raspberry Pi3, full-duplex master/slave bus. Figure 5 shows the device noise measured over 5 s, which is smaller than 0.1 μm and is about ± 3 of the least significant bit of the MCP3304.

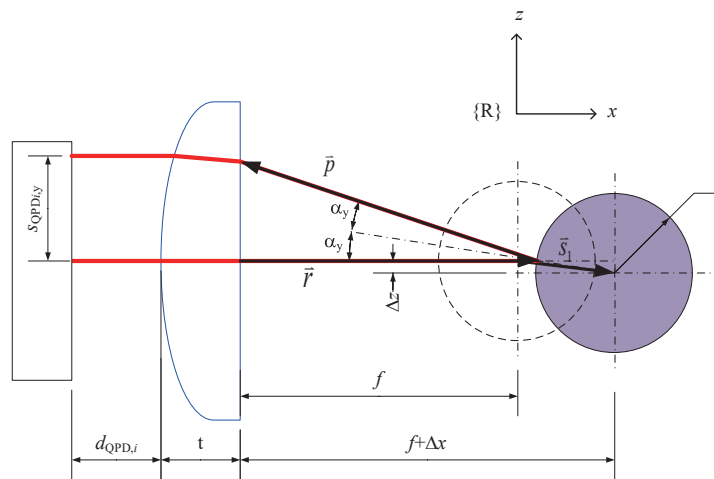


Fig. 3. (Color online) Mathematical model for the measurement modules.

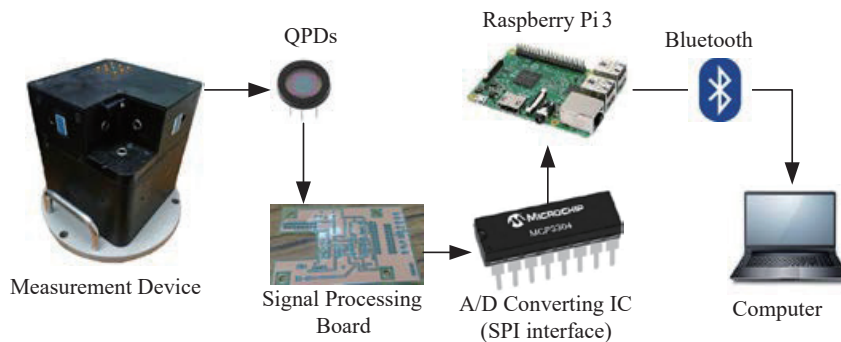


Fig. 4. (Color online) Signal processing schematic with measurement device.

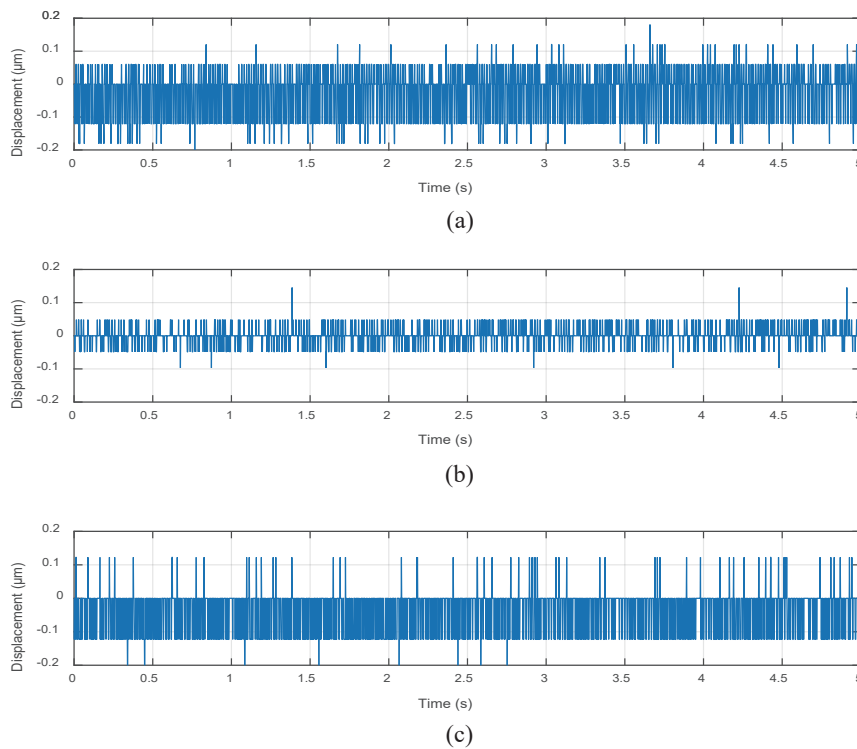


Fig. 5. (Color onlien) Device noise measured over 5 s: (a) x -, (b) y -, and (c) z -axes.

3. Experimental Results

3.1 Device calibration

Before measurements were performed, the device was carefully calibrated and the results are shown in Fig. 6. The measurement data was captured at a sampling rate of 1 kHz and 50 data points were averaged for each position. The conversion functions for QPD output voltage and spot displacement were

$$\begin{cases} x = 1.8505V_{QPD1,x}^2 + 52.549V_{QPD1,x}, \\ y = -0.0485V_{QPD2,x}^2 - 56.054V_{QPD1,x}, \\ z = 5.6702V_{QPD1,y}^2 - 110.73V_{QPD1,y}. \end{cases} \quad (5)$$

After voltage–displacement conversion, the residual error for the x -, y -, and z -axes was found to be less than 1 μm for a displacement of $\pm 50 \mu\text{m}$. The standard deviation (STDEV) for each measurement position was within a range of $\pm 0.2 \mu\text{m}$.

3.2 Spindle error motion

The setup for spindle error motion measurement is shown in Fig. 7. The measurement results, at a sampling rate of 1 kHz, for spindle speeds of 500 rev/min (about 8.3 Hz) and 100 rev/min

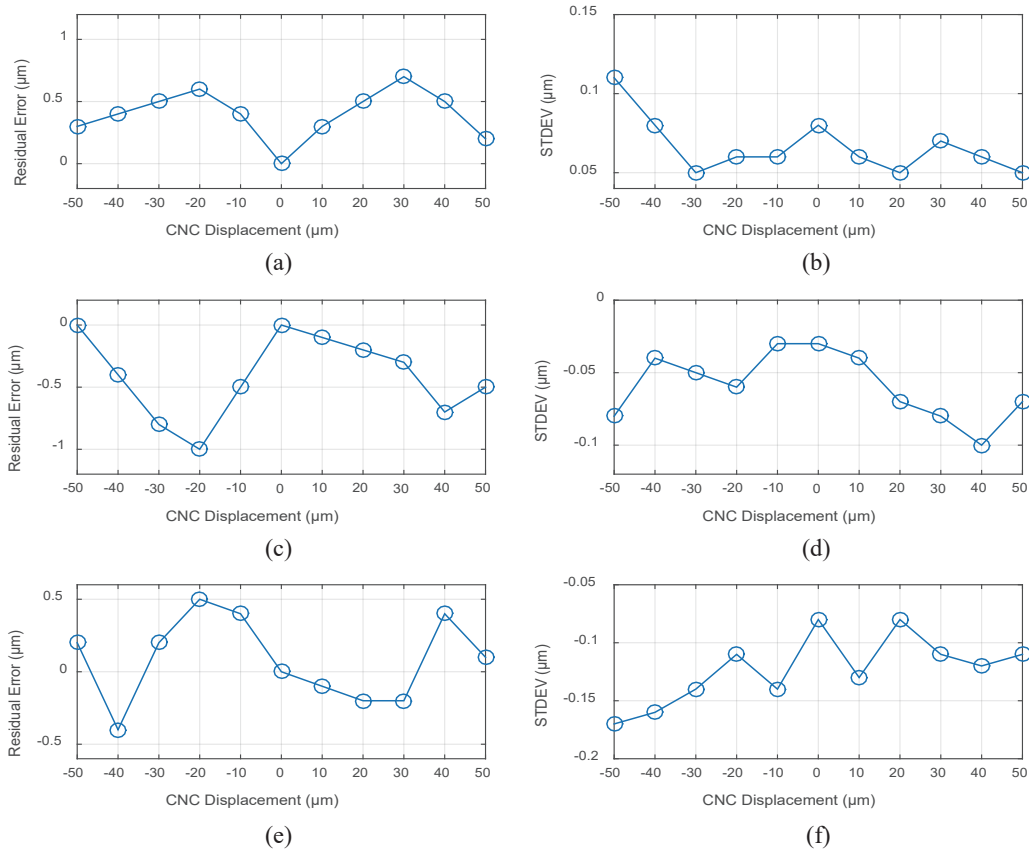


Fig. 6. (Color online) Calibration results for the measurement device: (a) x-axis residual error, (b) x-axis STDEV, (c) y-axis residual error, (d) y-axis STDEV, (e) z-axis residual error, and (f) z-axis STDEV.

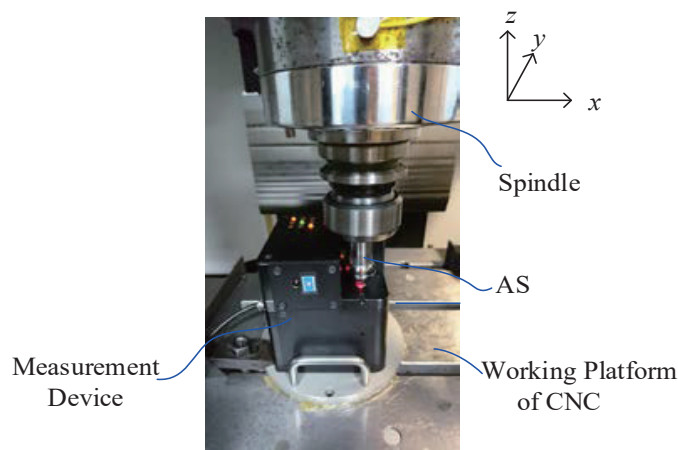


Fig. 7. (Color online) Setup for spindle error motion measurement.

(about 1.7 Hz) are shown in Fig. 8. The measurements include high-frequency noise on the x- and y-axes. After fast Fourier transformation (FFT), the vibration frequencies of the x- and y-axes were determined to be about 86.9 and 437.9 Hz, respectively (see Fig. 9). The number of vibration peaks

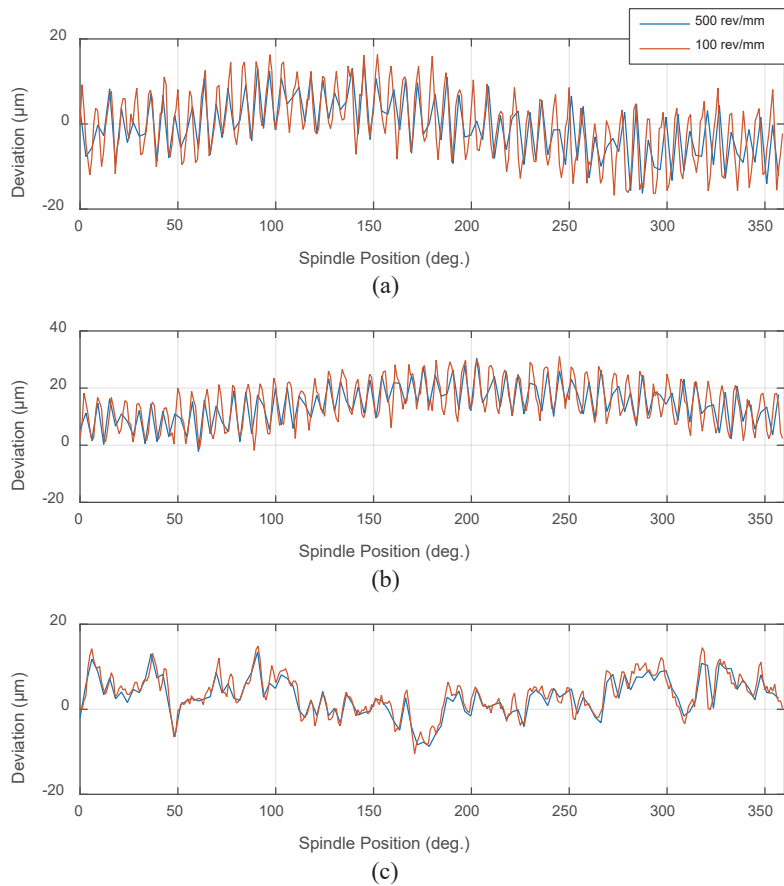


Fig. 8. (Color online) Spindle error motion measurements: (a) x-, (b) y-, and (c) z-axes.

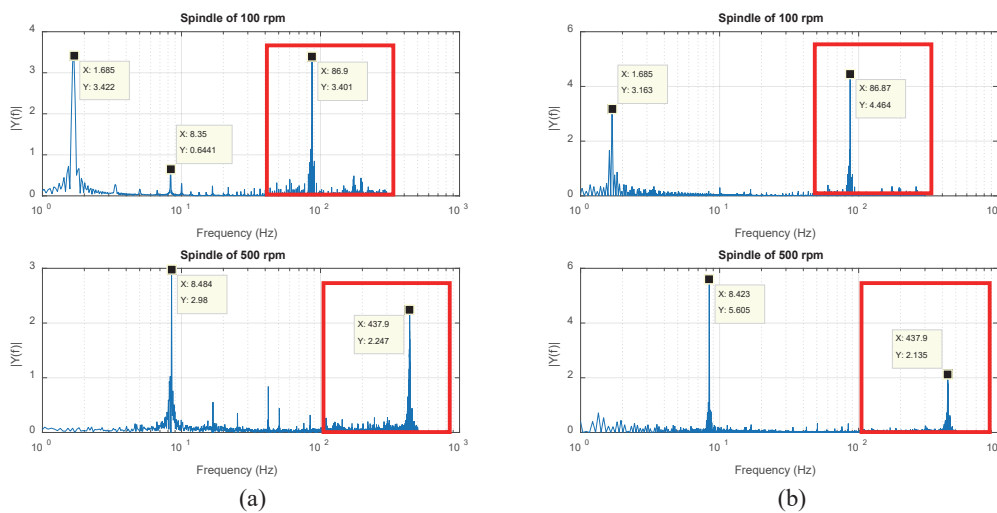


Fig. 9. (Color online) FFT of the spindle error motion measurement signal: (a) x- and (b) y-axes.

around the entire circumference of the sphere was counted and the results are shown in Figs. 8 and 10. We concluded that deviations in the curvature of the sphere caused the high-frequency measurement error. The measurement results were corrected by the removal of the high-frequency

signal and are shown in Fig. 11. Note that the number of data points recorded at 100 rev/min is larger than that at 500 rev/min because the same sampling rate was used for both measurements. After the high-frequency noise was removed, the synchronous and asynchronous errors of the spindle were determined and are shown in Fig. 12. The total error for the *xy*-plane and *z*-axis is shown in Fig. 13.

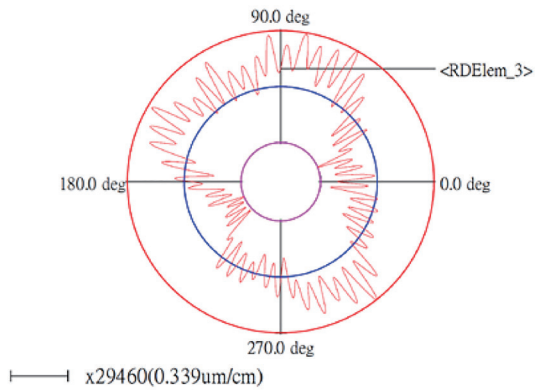
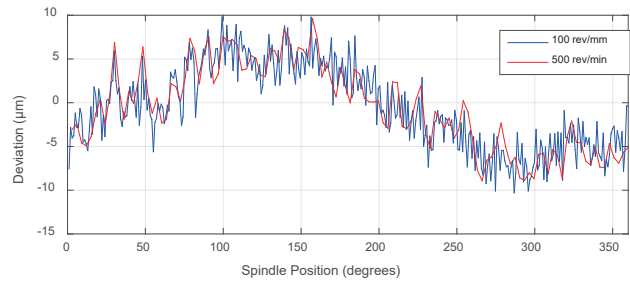
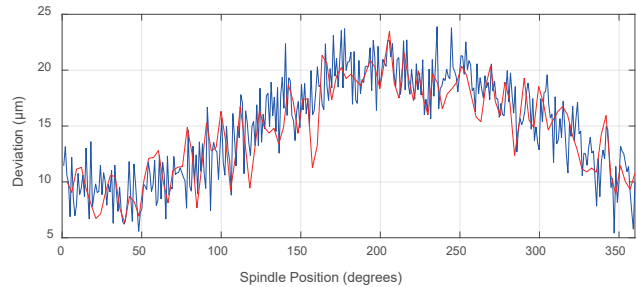


Fig. 10. (Color online) Roundness measurements of the AS sphere. The results show the roundness of the AS sphere to be about 0.7 μm .

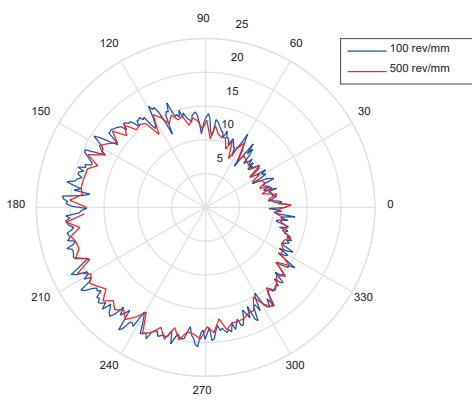


(a)

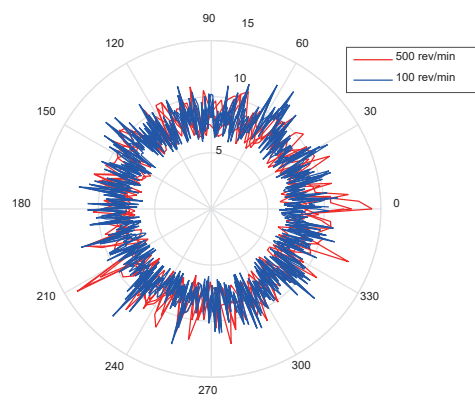


(b)

Fig. 11. (Color online) Measurement signal after high-frequency noise removal: (a) *x*- and (b) *y*-axes.



(a)



(b)

Fig. 12. (Color online) Measurement results after noise removal: (a) synchronous error, LSC center on $(-0.5, 14.9)$ and radius of $5.9 \mu\text{m}$ for 100 rev/min and LSC center on $(-0.8, 14.4)$ and radius of $5.9 \mu\text{m}$ for 500 rev/min and (b) asynchronous error (with a basic circle of $5.9 \mu\text{m}$ radius), and radius deviations smaller than 7 and $9 \mu\text{m}$ for 100 and 500 rev/min, respectively.

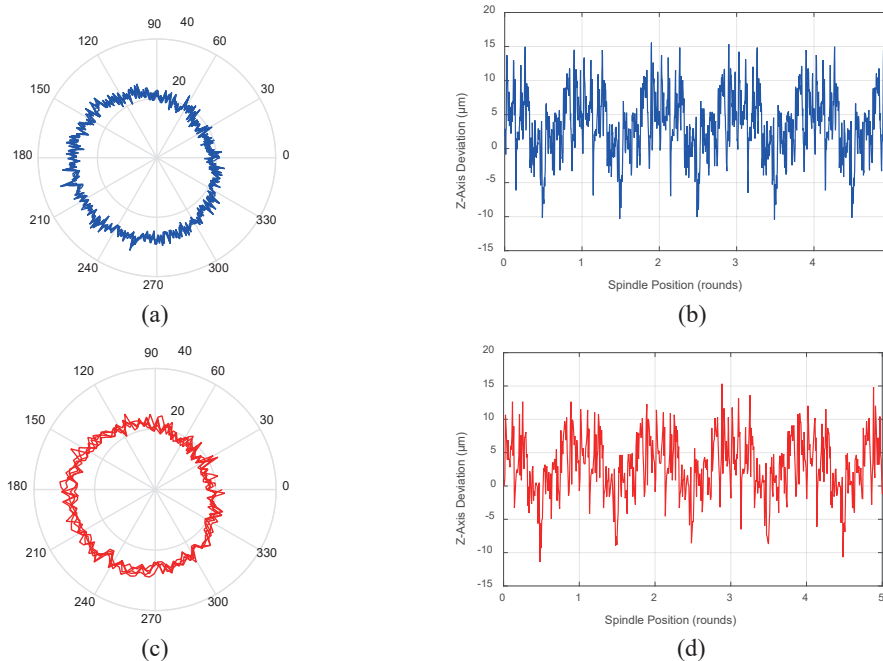


Fig. 13. (Color online) Total spindle error motion: (a) xy -plane at 100 rev/min, (b) z -axis at 100 rev/min, (c) xy -plane at 500 rev/min, and (d) z -axis at 500 rev/min.

4. Conclusions

An optical measurement device for spindle error motion measurement with 3DOF has been presented. The mathematical model shows that error motion for the x -, y -, and z -axes can be measured independently. The proposed measurement device is very simple and inexpensive. The results show that linear deviation and synchronous and asynchronous spindle error motion can all be measured. However, a high-frequency noise signal caused by deviations from the spherical curvature of the sphere is observed. The measurement results obtained clearly show that optical measurement modules can be applied and used for noncontact roundness measurement after accuracy and precision have been improved. The inexpensive spindle error motion measurement device, using a Raspberry Pi3 and a A/D converting IC (MCP 3304), was employed for measurement data acquisition. The integrated Bluetooth module allows the remote operation of the measurement device and also makes it possible to connect the device to the IoT. This makes the remote connection even more versatile. However, the stable sampling rate of the Raspberry Pi3 with the A/D converting IC is limited to a value less than 1 kHz by the internal clock of the Raspberry Pi3. This problem can be solved by using an external clock or a high-speed data acquisition card instead.

Acknowledgments

This work was supported by the Ministry of Science and Technology, Taiwan, under Grant Nos. MOST 105-2221-E-005-028, MOST 106-3114-8-005-003, and MOST 106-2218-E-005-003.

References

- 1 L. Chien-Hung, J. Wen-Yuh, and L. Hau-Wei: Meas. Sci. Technol. **15** (2004) 1733.
- 2 L. Jin, Z. Yan, L. Xie, W. Gou, and L. Tang: Int. J. Adv. Manuf. Technol. **70** (2014) 327.
- 3 E. Marsh, J. Couey, and R. Vallance: J. Manuf. Sci. Eng. **128** (2006) 180.
- 4 X. Lu, A. Jamalian, and R. Graetz: Precis. Eng. **35** (2011) 95.
- 5 P. D. Chapman: Precis. Eng. **7** (1985) 129.
- 6 X. Lu and A. Jamalian: Precis. Eng. **35** (2011) 73.
- 7 K. P. Anandan, A. S. Tulsian, A. Donmez, and O. B. Ozdoganlar: Precis. Eng. **36** (2012) 104.
- 8 H. F. F. Castro: Measurement **41** (2008) 526.
- 9 W. Gao, S. Kiyono, and T. Nomura: Precis. Eng. **19** (1996) 37.
- 10 K. P. Anandan and O. B. Ozdoganlar: Int. J. Mach. Tools Manuf. **70** (2013) 1.
- 11 H.-W. Lee, T.-P. Chiu, and C.-H. Liu: Sens. Mater. **28** (2016) 1053.
- 12 H.-W. Lee, C.-H. Liu, and W.-H. Lin: J. Chin. Soc. Mech. Eng. **35** (2014) 149.
- 13 H.-W. Lee and C.-H. Liu: Smart Sci. **4** (2016) 134.
- 14 Z. He, J. Fu, L. Zhang, and X. Yao: Int. J. Mach. Tools Manuf. **88** (2015) 1.
- 15 H.-W. Lee and C.-H. Liu: Rev. Sci. Instrum. **85** (2014) 095115.
- 16 Y.-H. Huang, C.-W. Huang, Y.-D. Chou, C.-C. Ho, and M.-T. Lee: Smart Sci. **4** (2016) 160.
- 17 T.-M. Jeng, S.-C. Tzeng, C.-W. Tseng, G.-W. Xu, and Y.-C. Liu: Smart Sci. **4** (2016) 38.
- 18 R. Jamuna, U. Natarajan, A. Elango, S. Jayavel, P. Gokulkumar, and V. Shakil: J. Adv. Manuf. Syst. **15** (2016) 27.
- 19 Y. Li, W. Zhao, S. Lan, J. Ni, W. Wu, and B. Lu: Int. J. Mach. Tools Manuf. **95** (2015) 20.
- 20 Z.-S. Yan, W.-H. Lin, and C.-H. Liu: Sens. Actuators, A **221** (2015) 154.

About the Authors



Hau-Wei Lee received his Ph.D. degree from the Institute of Aeronautics and Astronautics, National Cheng-Kung University, Taiwan, Republic of China, in 2010. From 2014 to 2017, he was a researcher at the Center for Measurement Standards, International Technology Research Institute, Taiwan. He is now a researcher at the Department of Mechanical Engineering, National Chung Hsing University, Taiwan. His main research fields are precision instrument design, dimension metrology, calibration of machine tools, and optomechatronic integration engineering.



Jr-Rung Chen completed his Ph.D. degree from National Taiwan University of Science and Technology, Taiwan, Republic of China, in 2010. He is working at the Center for Measurement Standards, International Technology Research Institute, Taiwan. His majors are dimension metrology, precision engineering, and mechatronics.



Bing-Lin Ho received his master's degree in 2016 from the Department of Mechanical Engineering, National Cheng-Kung University, Taiwan, Republic of China. He is a deputy engineer at the Center for Measurement Standards, International Technology Research Institute, Taiwan. His main research fields are kinematic analysis, robotic surgery, machine vision, dimension metrology, and MR-compatible design.



Chi-Chang Wang received his Ph.D. degree from the Department of Mechanical Engineering, National Cheng-Kung University, Taiwan, Republic of China, in 2000. He is now a professor at the Department of Mechanical and Computer-Aided Engineering, Feng-Chia University, Taiwan. His main research fields are heat inverse problem, numerical method, as well as heat and mass transfer analysis.